

1 **Measurement report: Chemical characteristics of PM_{2.5} during typical biomass**

2 **burning season at an agricultural site of the North China Plain**

3 Linlin Liang¹, Guenter Engling^{2,3}, Chang Liu¹, Wanyun Xu¹, Xuyan Liu⁴, Yuan Cheng⁵, Zhenyu

4 Du⁶, Gen Zhang¹, Junying Sun¹, Xiaoye Zhang¹

5 ¹ State Key Laboratory of Severe Weather & Key Laboratory for Atmospheric Chemistry, Chinese
6 Academy of Meteorological Sciences, Beijing 100081, China

7 ² Division of Atmospheric Sciences, Desert Research Institute, Reno, NV 89512, USA

8 ³ Now at: California Air Resources Board, El Monte, CA 91731, USA

9 ⁴ National Satellite Meteorological Center, Beijing 100081, China

10 ⁵ School of Environment, Harbin Institute of Technology, Harbin 150001, China

11 ⁶ National Research Center for Environmental Analysis and Measurement, Beijing 100029 China

12 **Abstract:**

13 Biomass burning activities are ubiquitous in China, especially in North China, where there is an
14 enormous rural population and winter heating custom. Biomass burning tracers (i.e., levoglucosan,
15 mannosan and potassium (K⁺)), as well as other chemical components were quantified at a rural site
16 (Gucheng, GC) in North China from 15 October to 30 November, during a transition heating season,
17 when the field burning of agricultural residues was becoming intense. The measured daily average
18 concentrations of levoglucosan, mannosan and K⁺ in PM_{2.5} during this study were $0.79 \pm 0.75 \mu\text{g}$
19 m^{-3} , $0.03 \pm 0.03 \mu\text{g m}^{-3}$ and $1.52 \pm 0.62 \mu\text{g m}^{-3}$, respectively. Carbonaceous components and biomass
20 burning tracers showed higher levels at nighttime than daytime, while secondary inorganic ions
21 were enhanced during daytime. An episode with high levels of biomass burning tracers was
22 encountered at the end of October, 2016, with high levoglucosan at $4.37 \mu\text{g m}^{-3}$. Based on the
23 comparison of chemical components during different biomass burning pollution periods, it appeared
24 that biomass combustion can obviously elevate carbonaceous components levels, whereas no
25 essentially effect on secondary inorganic aerosols in the ambient air. Moreover, the
26 levoglucosan/mannosan ratios during different biomass burning pollution periods remained at high
27 values (in the range of 18.3 - 24.9), however, the levoglucosan/K⁺ ratio was significantly elevated
28 during the intensive biomass burning pollution period (1.67) when air temperatures decreasing,

29 substantially higher than in other biomass burning periods (averaged at 0.47).

30 **Keywords:** Biomass burning; Organic tracers; Levoglucosan; Mannosan; Potassium

31 1. Introduction

32 Particulate air pollution is attracting more and more concerns in China because of their obvious
33 adverse impact on visibility reduction, as well as health implication and regional or global climate
34 change (Kanakidou et al., 2009; Pope and Dockery, 2006; Cheng et al., 2016). Carbonaceous species,
35 i.e., organic carbon (OC) and elemental carbon (EC), and water-soluble inorganic ions, e.g., SO_4^{2-} ,
36 NO_3^- and NH_4^+ are the major components of ambient aerosols (Liang et al., 2017; Du et al., 2014;
37 Zheng et al., 2015; Tan et al., 2016). Biomass burning (BB) emissions constitute a large source of
38 ambient particulate pollution, especially for carbonaceous components, i.e., primary organic carbon
39 (POC) and black carbon (BC) on global scale (Bond et al., 2004; Tang et al., 2018; Titos et al., 2017).

40 As an important aerosol component, black carbon from industrial and combustion emissions
41 contributes to the enhanced $\text{PM}_{2.5}$ (particulate matter with aerodynamic diameters less than $2.5 \mu\text{m}$)
42 mass concentrations and influences regional radiative forcing (Chen et al., 2017). Fresh biomass
43 burning aerosol was found to be mainly comprised of carbonaceous species which typically
44 constitutes 50-60% of the total particle mass (Hallquist et al., 2009). Yao et al. (2016) identified
45 approximately half of carbonaceous aerosols being contributed by biomass burning at Yucheng, a
46 rural site in the North China Plain.

47 Biomass burning emissions also represent a potentially large source of secondary organic
48 aerosol (SOA). The precursors and formation pathways of SOA from biomass burning emissions
49 were investigated by extensive field observations (e.g., Zhu et al., 2015; 2017; Adler et al., 2011;
50 Zhang et al., 2010; 2015). Based on morphological particle analysis, Yao et al. (2016) investigated
51 the smoke emitted from biomass burning impacting SOA production. Sun et al. (2010) found that
52 phenolic compounds, which were emitted in large amounts from wood combustion, can form SOA
53 at high yields in aqueous-phase reactions. In addition, smoke from biomass burning can be
54 transported thousands of kilometers downwind from the source areas. Biomass burning aerosol from
55 Southeast Asia can be transported to China, Singapore and even further to North America (Liang et
56 al., 2017; 2020; Hertwig et al., 2015; Peltier et al., 2008). Based on molecular tracer measurements,

57 synoptic data as well as air mass back trajectory analysis, a fire episode was captured at a
58 background site of East China with smoke advected from Southeast Asia (Liang et al., 2017).

59 The North China Plain (NCP) is one of the most polluted regions in China. Severe haze–fog of
60 longer duration and more extensive coverage has occurred frequently in the NCP area, especially
61 during the seasons of autumn and winter. NCP covers one quarter of China's cultivated land and
62 yields 35% of the agricultural products in China (Boreddy et al., 2017). The rural population in NCP
63 is also large and dense, and biomass burning activities are common in this region in form of cooking
64 and heating. Intense fire activity typically occurs in October after the corn harvest. Abundant smoke
65 is emitted from agricultural burning, i.e., residential biofuel combustion, open field burns, etc.
66 Various field observations have investigated different aspects of biomass burning, e.g., seasonal
67 variations, chemical and physical properties of smoke particles, spatial distribution, sources,
68 transport, etc., in the NCP region (Cheng et al., 2013; Shen et al., 2018; Sun et al., 2013; 2016;
69 Boreddy et al., 2017; Xu et al., 2019). However, these field investigations of the contribution of
70 biomass burning to ambient aerosols in the NCP region were concentrated on the city of Beijing
71 (Cheng et al., 2013; Zheng et al., 2015; Duan et al., 2004; Liang et al., 2016). Little field research
72 about biomass burning was reported for rural areas in the NCP. In fact, biomass burning activities
73 are common in the rural areas of the NCP region, and the resulting smoke aerosol can be transported
74 to urban areas, e.g., the city of Beijing, resulting in haze episodic events.

75 In order to characterize the biomass burning pollution status within rural areas of the NCP
76 region, multiple biomass burning tracers, i.e., levoglucosan, mannosan and K^+ in $PM_{2.5}$ sampled at
77 a heavily polluted rural site in Hebei province were quantified during a typical biomass burning
78 season, i.e., autumn-winter transition season, following the corn harvest. Combined with the
79 analysis of other chemical components, it reveals different levels of biomass combustion pollution
80 impacting on different types of chemical components in ambient aerosol. Meanwhile, based on the
81 multi-analysis of biomass burning molecular tracers, back trajectory analysis, fire activity data and
82 synoptic conditions, the results of this study demonstrate the biomass burning pollution status, as
83 well as the formation process of severe biomass burning pollution episode in the rural atmosphere
84 of North China. These results can provide valuable information about the biomass burning activities
85 in all of Northern China.

86 **2. Site description and experimental Methods**

87 **2.1 Site description and sampling**

88 Samples were collected at a rural site, Gucheng (GC, 39°09'N, 115°44'E; 15.2 m a.s.l), located
89 on a platform at the China Meteorological Administration farm in the town of Gucheng (GC site),
90 approximately 110 km southwest of Beijing and 35 km north of the city of Baoding (population of
91 about 5 million) in Hebei province, as shown in Figure S1. The station is surrounded by agricultural
92 fields, with major crop species being corn and wheat. The dominant wind direction at GC is
93 southwest and northeast during the study period. This site is upwind of Beijing, when the wind
94 blows from the south or southwest, where heavily polluted cities and regions of Hebei province, i.e.,
95 Baoding, Shijiazhuang, Xingtai, Handan, are located. Thus, it is an appropriate station for
96 representing the air pollution situation in the NCP region (Sheng et al., 2018; Chi et al., 2018; Xu
97 et al., 2019; 2020; Kuang et al., 2020).

98 Daytime and nighttime PM_{2.5} samples were collected from 15 October, 2016 to 23 November,
99 2016, by using PM_{2.5} High-volume (Hi-Vol) sampler (GUV-15HBL1, Thermo Fisher Scientific CO.,
100 LTD), at the nominal flow rate of 1.13 m³ min⁻¹. The daytime samples were collected from 07:00 to
101 19:00, while nighttime samples were collected from 19:00 to 07:00 local time of the next day. All
102 PM_{2.5} samples were collected on quartz fiber filters, prebaked at 850 °C for at least 5 h to remove
103 carbonaceous material. A total of 33 couples of daytime/nighttime samples and 6 whole-day samples
104 as well as 4 field blank samples were collected during the sampling period. The filters were stored
105 at -20 °C after sample collection.

106 **2.2 Experimental Methods**

107 **2.2.1 Anhydrosugar and water-soluble inorganic ion analysis**

108 The quartz filter samples were analyzed for biomass burning anhydrosugar tracers, i.e.,
109 levoglucosan and mannosan using an improved high-performance anion-exchange chromatography
110 (HPAEC) method with pulsed amperometric detection (PAD) on a Dionex ICS-5000+ system.
111 Levoglucosan and mannosan were separated by a Dionex CarboPac MA1 analytical column and
112 guard column with an aqueous sodium hydroxide (NaOH, 480 mM) eluent at a flow rate of 0.4 mL
113 min⁻¹. The detection limit of levoglucosan and mannosan was 0.002 mg L⁻¹ and 0.005 mg L⁻¹,

114 respectively. More details about the HPAEC-PAD method can be found elsewhere (Iinuma et al.,
115 2009).

116 The quartz filter samples were also analyzed for water-soluble inorganic ions by a Dionex ICS-
117 5000+ ion chromatograph, including SO_4^{2-} , NO_3^- , NH_4^+ , Cl^- , Ca^{2+} , Na^+ , K^+ and Mg^{2+} , and the
118 method detection limits for the individual ionic species were $0.18 \mu\text{g L}^{-1}$, $0.15 \mu\text{g L}^{-1}$, $0.03 \mu\text{g L}^{-1}$,
119 $0.048 \mu\text{g L}^{-1}$, $0.08 \mu\text{g L}^{-1}$, $0.01 \mu\text{g L}^{-1}$, $0.01 \mu\text{g L}^{-1}$, $0.008 \mu\text{g L}^{-1}$, respectively. The cations were
120 separated on an Ionpac CS12 analytical column and CG12 guard column with a 20 mM
121 methanesulfouic acid as eluent at a flow rate of 1.0 mL min^{-1} , while the anions were separated on
122 an Ionpac AS11-HC column and AG11-HC guard column with 21.5 mM KOH eluent at a flow rate
123 of 1.0 mL min^{-1} . The water-soluble inorganic ion data were corrected by field blanks.

124 **2.2.2 Organic carbon/elemental carbon analysis**

125 OC and EC were measured on a punch (0.526 cm^2) of each quartz sample by a thermal/optical
126 carbon analyzer (DRI Model 2001, Desert Research Institute, USA), using the Interagency
127 Monitoring of Protected Visual Environments (IMPROVE) thermal evolution protocol with
128 reflectance charring correction. The analytical error of OC was within 10%, and one sample of every
129 10 samples was selected at random for duplicate analysis. The detection limit of OC was $0.82 \mu\text{g C}$
130 cm^{-2} (Liang et al., 2017).

131 **2.2.3 Gas online monitoring (i.e., NO, NO₂, SO₂, O₃, CO and NH₃)**

132 During this campaign, commercial instruments from Thermo Fisher Scientific Co., LTD were
133 used to measure O₃ (TE 49C), NO/NO₂/NO_x (Model 42CTL), CO (TE 48CTL), and SO₂
134 (TE43CTL), while NH₃ was measured by an ammonia analyzer (DLT-100, Los Gatos Research,
135 USA) at GC station. All measurement data quality was controlled according to standard gases (Xu
136 et al., 2019; Lin et al., 2011; Meng et al., 2018; Ge et al., 2018).

137 **2.2.4 Meteorological parameters**

138 The meteorological parameters, including air temperature, relative humidity (RH) and wind
139 speed at a 24-h resolution at the GC site are presented in Figure 1. During this campaign, the daily
140 average RH value was observed at $77 \pm 13\%$, with a range from 48% to 99%, while the daily wind
141 speed was observed with an average value of $1.07 \pm 1.14 \text{ m s}^{-1}$, exhibiting moist and stable synoptic
142 conditions at this rural site during the autumn-winter transition season. Moreover, there was rare

143 precipitation during the sampling period at the GC site, except for two days, i.e., 20 and 27 October,
144 2016 (Figure 1).

145 **2.2.5 Back trajectory and fire spot analysis**

146 To characterize the transport pathways of the aerosol at the Gucheng site, back-trajectories
147 were calculated with the NOAA Hybrid Single-Particle Lagrangian Integrated Trajectory
148 (HYSPLIT) model via NOAA ARL READY Website (<http://ready.arl.noaa.gov/HYSPLIT.php>).

149 To investigate the influence of biomass burning activities in surrounding areas, fire hot spot
150 counts were obtained from the Fire Information for Resource Management System (FIRMS)
151 (available at <https://firms.modaps.eosdis.nasa.gov/download/>).

152 **2.2.6 Statistical analysis**

153 Statistical analysis of data, i.e., the correlation analysis between the concentrations of
154 levoglucosan, mannosan and K⁺ at the Gucheng site during the sampling period were conducted
155 with the linear fitting method.

156 **3. Results and discussion**

157 **3.1 Characteristics of chemical components in PM_{2.5}**

158 In this study, the mass concentration of PM_{2.5-cal} was reconstituted by the sum of carbonaceous
159 components (1.6×OC + EC) and inorganic ions (SO₄²⁻ + NH₄⁺ + NO₃⁻ + Cl⁻ + Ca²⁺ + Na⁺ + K⁺ +
160 Mg²⁺). Figure 1 describes the time-series variation obtained for daily PM_{2.5-cal}, OC, EC, biomass
161 burning tracers (levoglucosan, mannosan and K⁺), ratios of levoglucosan/OC and meteorological
162 factors (temperature, RH, wind speed and planetary boundary layer (PBL) height) during the
163 sampling period. The average daily PM_{2.5-cal} mass concentration in the autumn-winter transition
164 season at GC reached $137 \pm 72.4 \mu\text{g m}^{-3}$, ranging from $23.3 \mu\text{g m}^{-3}$ to $319 \mu\text{g m}^{-3}$ (Table 1, Figure
165 1a), which is higher than during the severe winter haze in January, 2013 at an urban site in Beijing
166 ($121 \mu\text{g m}^{-3}$) (Zheng et al., 2015). The mass concentrations of these chemical species during the day
167 are distributed as follows (from highest to lowest): OC > EC > NO₃⁻ > SO₄²⁻ > NH₄⁺ > Cl⁻ > Ca²⁺ >
168 K⁺ > Na⁺ > Mg²⁺. Organic matter (OM), calculated by multiplying OC values with a coefficient of
169 1.6, was the most abundant PM component, the daily average value of which was $70.4 \pm 49.6 \mu\text{g}$
170 m^{-3} , accounting for nearly half (46.7%) of PM_{2.5-cal} mass, indicating obvious organic pollution at

171 the rural site in the North China Plain during the sampling season.

172 The measured daily average concentrations of biomass burning tracers, i.e., levoglucosan,
173 mannosan and K^+ in $PM_{2.5}$ during our study were $0.79 \pm 0.75 \mu g m^{-3}$, $0.03 \pm 0.03 \mu g m^{-3}$ and $1.52 \pm$
174 $0.62 \mu g m^{-3}$, respectively (Table 1). The ambient concentrations of levoglucosan in this study were
175 higher than those observed in the city of Beijing during the summer (averaged at $0.23 \pm 0.37 \mu g m^{-3}$,
176 in the range of 0.06 to $2.30 \mu g m^{-3}$) and winter (averaged at $0.59 \pm 0.42 \mu g m^{-3}$, in the range of
177 0.06 to $1.94 \mu g m^{-3}$) of 2010-2011 (Cheng et al., 2013). The biomass burning tracer levels and ratios
178 observed in this study and other field studies are summarized in Table S1. The highest
179 concentrations of levoglucosan in GC were observed on 31 October, 2016 with $4.37 \mu g m^{-3}$, which
180 is a sharp increase (over 30 times) of the minimum concentration ($0.14 \mu g m^{-3}$) during that period
181 (Figure 1c). Accordingly, the $PM_{2.5-cal}$ concentration during that period was also elevated (as high
182 as $236 \mu g m^{-3}$) (Figure 1a). Secondary inorganic aerosol (sulfate, SO_4^{2-} ; nitrate, NO_3^- and
183 ammonium, NH_4^+ , SNA) species, were the major water soluble ions, accounting for 82.8% of total
184 water soluble ions, the daily average values of which were $10.5 \pm 6.87 \mu g m^{-3}$, $15.9 \pm 9.29 \mu g$
185 m^{-3} and $10.9 \pm 5.51 \mu g m^{-3}$, respectively (Table 1). SNA species exhibited a synchronous temporal
186 trend (Figure 1c), while the NO_3^- concentrations exceeded those of SO_4^{2-} at the GC site, in contrast
187 to the results of previous studies, e.g., Tan et al. (2016), who found SO_4^{2-} to be the dominant species
188 in $PM_{2.5}$ during winter in 2006 in Beijing. Similarly, Chi et al., (2018) also found
189 NO_3^- concentrations exceeded those of SO_4^{2-} at both Beijing and GC sites during the winter in 2016,
190 although they observed that NH_4^+ was the dominant component of SNA (the concentrations of
191 SO_4^{2-} , NO_3^- and NH_4^+ were $14.0 \mu g m^{-3}$, $14.2 \mu g m^{-3}$, and $24.2 \mu g m^{-3}$, respectively).

192 **3.2 Day-night variations in the characteristics of $PM_{2.5}$ chemical components**

193 Carbonaceous components and biomass burning tracers exhibited higher levels during
194 nighttime than daytime, while secondary inorganic ions showed the opposite pattern, i.e., higher
195 concentrations during daytime than nighttime (Figure 2 and Figure S2). Besides, the gap of
196 carbonaceous components and anhydrosugars between daytime and nighttime (two-fold) was more
197 significant than for secondary inorganic ions. EC, POC are not subject to significant differences in
198 chemical reactions in ambient air between daytime and nighttime, and they will be mainly
199 influenced by the variations of the PBL height. In the night, the PBL height decreases, compressing

200 air pollutants into a shallow layer, and subsequently resulting in faster accumulation and higher
201 concentrations of pollutants (Zheng et al., 2015; Zhong et al., 2018; 2019). The contributions of OM
202 and EC to PM_{2.5-cal} were observed to be higher at nighttime (53.9% and 16.6%) than daytime (43.8%
203 and 13.7%) as well (Figure 3). Besides the influence from variations of the PBL height, the chemical
204 degradation of levoglucosan may occur due to photochemical reaction in the ambient aerosols
205 during daytime, further enlarging the gap of levoglucosan levels between daytime and nighttime
206 (Sang et al., 2016; Gensch et al., 2018). Consequently, the contribution of levoglucosan to PM_{2.5-cal}
207 during daytime (0.45%) was observed to be considerably lower than that during nighttime (0.64%)
208 (Figure 3). However, secondary inorganic ions have an important formation pathway, i.e.,
209 photochemical processing, during daytime. Thus, the secondary inorganic species (SO₄²⁻, NO₃⁻ and
210 NH₄⁺) were enhanced during daytime due to photochemical formation (Sun et al., 2013; Zheng et
211 al., 2015; Wu et al., 2018). The mass contributions of SO₄²⁻, NO₃⁻ and NH₄⁺ to PM_{2.5-cal} were
212 decreased from daytime (9.9%, 14.5% and 10.0%) to nighttime (6.5%, 9.6% and 7.1%) (Figure 3).
213 Such an enhancement in secondary transformations during daytime is more evident in terms of the
214 sulfur and nitrogen oxidation ratios (SOR and NOR, molar ratio of sulfate or nitrate to the sum of
215 sulfate and SO₂ or nitrate and NO₂), which have been used previously as indicators of secondary
216 transformations (Sun et al., 2013; Zheng et al., 2015). Both SOR and NOR during daytime were
217 higher than those during nighttime (Figure S3), further confirming the elevated secondary
218 formations of sulfate and nitrate during daytime.

219 In addition, the concentrations of other water-soluble inorganic ions, i.e., K⁺ and Cl⁻ during
220 nighttime ($1.78 \pm 0.95 \mu\text{g m}^{-3}$ and $6.08 \pm 4.00 \mu\text{g m}^{-3}$) were higher than those in daytime ($1.43 \pm$
221 $0.54 \mu\text{g m}^{-3}$ and $4.33 \pm 2.30 \mu\text{g m}^{-3}$), while their contributions to PM_{2.5-cal} were reversed, due to the
222 significant accumulation and higher concentrations of pollutants during nighttime. As Ca²⁺, Mg²⁺
223 and Na⁺, mainly emitted from primary natural sources, such as dust, soil resuspension and sea salt,
224 are subject to more activity during the daytime and also influenced by the airflow dynamics, the
225 contribution of those species in nighttime were lower than those during daytime, especially for Ca²⁺,
226 decreasing from 2.2% in daytime to 0.9% at nighttime (Figure 3).

227 **3.3 Biomass burning episodes and the impacts on chemical PM_{2.5} characteristics**

228 An episode with high biomass burning tracer levels was encountered on 31 October, 2016.

229 The concentrations of levoglucosan in $\text{PM}_{2.5}$ during this one-day episode ($4.37 \mu\text{g m}^{-3}$) were
230 significantly higher than those during typical transition season at the GC site ($0.69 \pm 0.47 \mu\text{g m}^{-3}$)
231 (Figure 1d). Meanwhile, there was significant change in the meteorological conditions, i.e., the wind
232 direction changed from southwesterly to northerly winds (Figure S4). Northerly winds advected
233 cold and dry air masses, with the lowest hourly temperature observed at -5.3°C (Figure S5). This
234 notable temperature decline before the commencing of the operation of the central heating systems
235 should have caused intense combustion activities for heating purposes at the rural site. Moreover,
236 the synoptic situation on 31 October, 2016 was under weaker turbulence with low PBL height and
237 small wind speeds (Figure 1f). These worsened meteorological conditions would further enhance
238 aerosol accumulation.

239 Here, we mainly distinguish four sub-periods based on daily levoglucosan concentrations
240 during the time frame from 15 October to 23 November, 2016. The four periods were separated as
241 follows: 15-30 October (Period I: Minor biomass burning), 31 October (Period II: Intensive biomass
242 burning), 1-14 November (Period III: Major biomass burning), 15-23 November (Period IV:
243 Heating season). Table 2 compares the concentrations of $\text{PM}_{2.5\text{-cal}}$ mass, chemical components and
244 gases at the GC site during these four periods, as well as the ratios between the intensive, major BB
245 periods and heating season to minor BB period. The level of levoglucosan during the intensive BB
246 episode II was about 12 times of that during the minor BB period I. K^+ and Cl^- , the common biomass
247 burning tracers utilized in many studies (Duan et al., 2004; Cheng et al., 2013), were also observed
248 with increased abundance during intensive BB episode II. When entering into November, the
249 weather was becoming cold, and thus combustion activities for heating in the rural areas commenced,
250 resulting in the ambient levels of levoglucosan to increase to $0.92 \pm 0.47 \mu\text{g m}^{-3}$ during period III,
251 about 3 times of those in Period I. The central heating systems in North China cities were operated
252 during period IV, and the ambient level of levoglucosan was observed at $0.96 \pm 0.63 \mu\text{g m}^{-3}$, which
253 was similar to that observed in period III.

254 The concentrations of OC and EC were also observed to be strongly elevated in period II (Table
255 2), and especially OC levels increased to $96.3 \mu\text{g m}^{-3}$ during the intensive BB episode II, nearly 6
256 times of those during the minor BB period ($16.2 \pm 7.52 \mu\text{g m}^{-3}$). The levoglucosan/OC ratio was
257 utilized to estimate the effect of biomass burning to ambient organic aerosols. Accordingly,

258 levoglucosan/OC ratios sharply increased to 0.045 during period II, which was noticeably higher
259 than during other periods in this study (Figure 1e). Moreover, this level is also higher than most of
260 the published field observations, i.e., at urban sites (Zhang et al., 2008; Cheng et al., 2013; Zhang
261 et al., 2014), rural sites (Sang et al., 2013; Ho et al., 2014; Pietrogrande et al., 2015; Mkoma et al.,
262 2013) and agricultural sites (Ho et al., 2014; Jung et al., 2014), yet lower than at an urban site in
263 northern Italy during winter time (in the range of 0.01 to 0.13) (Pietrogrande et al., 2015). This
264 illustrates that biomass combustion played an important role in organic aerosol pollution during the
265 intensive BB episode II. However, due to other emissions of OC enhanced during the major BB
266 episode (period III) and heating season (period IV), i.e., combustion of coal and biofuel for heating,
267 OC increased to a higher level ($55.2 \pm 17.1 \mu\text{gC m}^{-3}$ and $69.4 \pm 24.6 \mu\text{gC m}^{-3}$, respectively). Due to
268 the abundance of organic aerosols, the contribution from biomass burning emission was thereby
269 reduced and the levoglucosan/OC ratios during periods III and IV decreased to 0.016 ± 0.005 and
270 0.014 ± 0.006 , respectively, even lower than those observed in the minor BB period I (0.025 ± 0.008).

271 Compared to the carbonaceous components, the concentrations of secondary inorganic aerosol
272 species (SO_4^{2-} , NO_3^- , NH_4^+) exhibited a different pattern, i.e., showing no obvious differences
273 between minor BB period I and other three periods. The ratios of SO_4^{2-} , NO_3^- , NH_4^+ during periods
274 II, III and IV to period I were all around 1.0 (Table 2), with no increasing trend. Moreover, the
275 relationships between levoglucosan and OC (and EC) were better than those between levoglucosan
276 and SNA during daytime and nighttime (Figure S3). The precursor gases of SNA, i.e., SO_2 , NO ,
277 NO_2 and NH_3 , were observed to have an increasing trend when biomass burning was prevalent
278 during periods III and IV, with the ratios to period I arranged from 1.13 to 1.90 (Table 2). The time-
279 series variations of the gases (SO_2 , NO_x , NH_3 , CO and O_3) and PBL during the sampling period
280 are shown in Figure S4. The primary emission gases were exhibited negative relationships with PBL,
281 while O_3 exhibited obvious positive relationship with PBL (Figure S5). Combustion from different
282 fossil fuels (coal, gasoline, diesel, etc.) and biomasses (straws, woods, leaves, etc.) can all emit CO
283 into the atmosphere (Streets et al., 2003; Chantara et al., 2019; Merico et al., 2020). Due to the more
284 abundant combustion in the colder weather, the concentrations of CO also increased to 1.65 ± 0.53
285 ppm and 1.18 ± 0.83 ppm during the major biomass burning period III and the heating season period
286 IV, respectively.

287 The combustion of biomass, especially of agricultural residues (e.g., wheat and corn straw) is
288 very common in the rural areas in North China during the autumn-winter transition period. During
289 the autumn harvest season in North China, wheat and corn straw burning is common practice,
290 resulting in more abundant fire spots when entering into November than period I (Figure 4). The
291 intense biomass burning event on 31 October, 2016 was also supported by air mass back trajectory
292 analysis (Figure 5), performed with the TrajStat software. Based on the 48 h back trajectories at the
293 GC site at 00:00 (UTC time) on 1 November, 2016, the air mass at the GC site was restricted in the
294 region of Bejing-Tianjing-Hebei, the polluted area where fire spots were numerous. However, on
295 the previous and following day of this episode, i.e., 31 October and 2 November onward, the air
296 masses arriving at GC were advected from the northwest of Mongolia, where mostly desert areas
297 are present, with less farm land and rare biomass burning activities (Figure 5).

298 Mean percentiles of major components in $PM_{2.5}$ with respect to different BB pollution periods
299 at GC site during the sampling time are shown in Figure 6. With the variation of BB pollution
300 periods, the EC fraction seems to exhibit no obvious change during periods I, II and III, but slightly
301 increased during the heating season (period IV), while the OC fraction increased significantly from
302 34.0% during the minor BB period I elevated to 65.4% during the intense BB period II. The
303 contributions of sulfate, nitrate and ammonium to $PM_{2.5-cal}$ all decreased sharply from the minor BB
304 period to the intense period (Figure 6). This suggests that organic aerosol species become more
305 important during BB pollution periods, concerning their contribution to the $PM_{2.5-cal}$, while EC has
306 no such character. The OM percentage during intense BB period II was 65.4%, about double of that
307 during the minor biomass burning period (34.0%), indicating that there was a large fraction of OM
308 in $PM_{2.5-cal}$ originating from BB at the GC site during intensive BB period II. Opposite to OM,
309 contributions of secondary inorganic ions to $PM_{2.5-cal}$ significantly decreased with the BB pollution
310 becoming more severe. The contributions of SO_4^{2-} , NO_3^- and NH_4^+ to $PM_{2.5-cal}$ during the minor
311 BB episode (11.6%, 20.5% and 12.5%) obviously declined during the intense BB episode (1.93%,
312 7.67% and 4.24%).

313 **3.4 Relationships among tracers during different biomass burning pollution
314 periods**

315 In addition to pollution level information of biomass burning molecular tracers, the ratios
316 between them could also be used to identify the different biomass types or indicate the burning
317 formation processes of atmospheric aerosols. Levoglucosan and mannosan showed a good
318 relationship during the entire sampling period (Figure 7a, $r = 0.97$, $p < 0.01$). The
319 levoglucosan/mannosan ratios during minor, intense, major biomass pollution and heating season
320 periods were observed at high values, i.e., 24.9, 24.1, 24.8 and 18.3 respectively (Table 2, Figure 7).
321 Compared to the former three episodes (24.1 to 24.9, averaged at 24.6), the levoglucosan/mannosan
322 ration during the heating season period (18.3) decreased by 25.6%. Based on source emission studies,
323 the levoglucosan/mannosan ratios from crop residue burning, i.e., rice straw, wheat straw and corn
324 straw, are similar and are characterized by high values (averaged at 29, in the range of 12 to 55)
325 (Zhang et al., 2007; Engling et al., 2009; Cheng et al., 2013; Jung et al., 2014), yet overlapping with
326 those from hardwood (averaged at 28, in the range of 11 to 146) (Bari et al., 2009; Jung et al., 2014)
327 and grass burning (18.2 ± 10.2) (Sullivan et al., 2008), while softwood is characterized by relatively
328 lower levoglucosan/mannosan ratios (averaged at 4.3, in the range of 2.5 to 4.7) (Engling et al.,
329 2006; Cheng et al., 2013; Jung et al., 2014). Subsequently, this declining trend in the
330 levoglucosan/mannosan ratios during the heating season period was partly caused by the higher
331 proportion of softwood combustion, which is characterized by relatively lower
332 levoglucosan/mannosan ratios. According to the local habits, soft woods, e.g. China fir and pine are
333 also commonly used as biofuels for stove heating in North China, since they allow sustained heating
334 duration.

335 The concentrations of levoglucosan and K^+ during minor, major BB episode and heating season
336 were correlated well (Figure 7b, $r = 0.84$, $p < 0.01$), while the red dot of period II being off from the
337 fitted regression line. The levoglucosan/ K^+ ratios during periods III and IV (0.51 and 0.53) were
338 similar to those during a BB episode at an urban site in Beijing during winter time
339 (levoglucosan/ $K^+ = 0.51$) (Cheng et al., 2013). However, the levoglucosan/ K^+ ratio during the
340 intense BB period II increased to 1.67, which was significantly higher than that in typical straw
341 combustion (< 1.0). Correspondingly, there was a significant drop in temperatures at the GC site

342 during period II, with the average daily temperature sharply decreasing from 7.5 °C on 30 Oct to
343 0.31 °C on 31 October, 2016, and the average temperature at night of 31 October even decreased to
344 -3.4 °C (Figure 1g). Hence, the combustion activities were apparently intense around the sampling
345 site for heating purposes. Compared to K⁺, there is a large enrichment of levoglucosan in wood
346 burning emissions, based on the results from previous biomass source combustion studies (Engling
347 et al., 2006; Chantara et al., 2019). The influence of softwood and/or other materials from softwood,
348 which are commonly used as biofuels for stove heating in North China (Cheng et al., 2013; Zhou et
349 al., 2017), should be larger during this low temperature period. Moreover, levoglucosan/K⁺ ratios
350 also can be influenced by combustion conditions, i.e., smoldering versus flaming burns. Biofuels
351 are typically subject to smoldering combustion condition in residential stoves for heating purposes
352 in the rural areas in North China, which was reflected in relatively higher levoglucosan/K⁺ ratios
353 than during flaming combustion (Schkolnik et al., 2005; Lee et al., 2010).

354 **4. Summary and conclusion**

355 Anhydrosugars, including levoglucosan and mannosan, and water-soluble potassium ion were
356 employed as molecular tracers to investigate the characteristics of biomass burning activities as well
357 as chemical properties of ambient aerosols under different biomass burning pollution levels. The
358 measured daily average concentrations of levoglucosan, mannosan and K⁺ in PM_{2.5} during a typical
359 biomass burning season from 15 October to 30 November, 2016 were $0.79 \pm 0.75 \mu\text{g m}^{-3}$, $0.03 \pm$
360 $0.03 \mu\text{g m}^{-3}$ and $1.52 \pm 0.62 \mu\text{g m}^{-3}$, respectively. The concentrations of carbonaceous components
361 and biomass burning tracers were observed higher at nighttime than daytime, while the patterns of
362 secondary inorganic ions (SO₄²⁻, NO₃⁻ and NH₄⁺) were opposite, since they were enhanced by
363 photochemical formation during daytime. An episode with extreme biomass burning tracer levels
364 was encountered on 31 October, 2016, with concentrations of levoglucosan as high as $4.37 \mu\text{g m}^{-3}$.
365 Comparing the chemical compositions between different biomass burning periods, it was apparent
366 that biomass burning can considerably elevate the levels of organic components, while not showing
367 a significant effect on the production of secondary inorganic ions. Compared to the other biomass
368 burning episodes, the levoglucosan/mannosan ratios during the heating season period slightly
369 decreased, while levoglucosan/K⁺ ratio during the intensive BB period was unusually higher than
370 those in the other three biomass burning periods.

371

372 **Data availability.** The data used in this study can be obtained from this open
373 link: <https://pan.baidu.com/s/11bKUZff1KJbzNVxS3VsLaA> code: jvqx. It is also available from
374 the corresponding author upon request (lianglinlin@cma.gov.cn).

375 **Author contributions.** LL designed conducted all observations and drafted the paper. GE revised
376 the paper and improved the English writing. XL drew the Figure 4 and Figure 5. CL, WX, YC, ZD,
377 GZ, JS and XZ interpreted the data and discussed the results. All authors approved the final version
378 for publication.

379 **Competing interests.** The authors declare that they have no conflict of interest.

380 **Special issue statement.** This article is part of the special issue “In-depth study of air pollution
381 sources and processes within Beijing and its surrounding region (APHH-Beijing) (ACP/AMT
382 interjournal SI)”. It is not associated with a conference.

383 **Acknowledgements.** This research is supported by the Beijing Natural Science Foundation
384 (8192055) and CAMS Fundamental Research Funds (No. 2017Z011). The authors would like to
385 acknowledge Yingli Yu and Ye Kuang for their help with PM_{2.5} samples collection; Hongbing
386 Cheng for help with chemical analyses.

387 **Financial support.** This research has been supported by the Beijing Natural Science Foundation
388 (No. 8192055), State Environmental Protection Key Laboratory of Sources and Control of Air
389 Pollution Complex (No. SCAPC201701) and Chinese Academy of Meteorological Sciences
390 Fundamental Research Funds (No. 2017Z011).

391 **References:**

392 Bari, M. A., Baumbach, G., Kuch, B., and Scheffknecht, G.: Wood smoke as a source of particle-
393 phase organic compounds in residential areas, *Atmos. Environ.*, 43, 4722-4732,
394 <https://doi.org/10.1016/j.atmosenv.2008.09.006>, 2009.

395 Boreddy, S. K. R., Kawamura, K., Okuzawa, K., Kanaya, Y., and Wang, Z.: Temporal and diurnal
396 variations of carbonaceous aerosols and major ions in biomass burning influenced aerosols
397 over Mt. Tai in the North China Plain during MTX2006, *Atmos. Environ.*, 154, 106-
398 117, <http://dx.doi.org/10.1016/j.atmosenv.2017.01.042>, 2017.

399 Caseiro, A., Bauer, H., Schmidl, C., Pio, C. A., and Puxbaum, H.: Wood burning impact on PM₁₀ in
400 three Austrian regions, *Atmos. Environ.*, 43, 2186-
401 2195, <https://doi.org/10.1016/j.atmosenv.2009.01.012>, 2009.

402 Chantara, S., Thepnuan, D., Wiriya, W., Prawan, S., and Tsai, Y.I.: Emissions of pollutant gases,

403 fine particulate matters and their significant tracers from biomass burning in an open-system
404 combustion chamber, Chemos. 224, 407-
405 416, <https://doi.org/10.1016/j.chemosphere.2019.02.153>, 2019.

406 Cheng, Y., He, K.B., Du, Z.Y., Engling, G., Liu, J.M., Ma, Y.L., Zheng, M., Weber, R.J.: The
407 characteristics of brown carbon aerosol during winter in Beijing, Atmos. Environ., 127, 355-
408 364, <https://doi.org/10.1016/j.atmosenv.2015.12.035>, 2016.

409 Cheng, Y., Engling, G., He, K.B., Duan, F.K., Ma, Y.L., Du, Z.Y., Liu, J.M., Zheng, M., and Weber,
410 R.J.: Biomass burning contribution to Beijing aerosol, Atmos. Chem. Phys., 13, 7765-
411 7781, <https://doi.org/10.5194/acp-13-7765-2013>, 2013.

412 Chi, X., He, P., Jiang, Z., Yu, X., Yue, F., Wang, L., Li, B., Kang, H., Liu, C., and Xie, Z.: Acidity
413 of aerosols during winter heavy haze events in Beijing and Gucheng, China, J. Meteorol. Res.,
414 32, 14-25, <https://doi.org/10.1007/s13351-018-7063-4>, 2018.

415 Drewnick, F., Hings, S. S., Curtius, J., Eerdekens, G., and Williams, J.: Measurement of fine
416 particulate and gas-phase species during the New Year's fireworks 2005 in Mainz, Germany,
417 Atmos. Environ., 40, 4316-4327, <https://doi.org/10.1016/j.atmosenv.2006.03.040>, 2006.

418 Du, Z.Y., He, K.B., Cheng, Y., Duan, F.K., Ma, Y. L., Liu, J.M., Zhang, X.L., Zheng, M., and Weber,
419 R.: A yearlong study of water-soluble organic carbon in Beijing I: Sources and its primary vs.
420 secondary nature, Atmos. Environ., 92, 514-
421 521, <https://doi.org/10.1016/j.atmosenv.2014.04.060>, 2014.

422 Duan, F., Liu, X., Yu, T., and Cachier, H.: Identification and estimate of biomass burning
423 contribution to the urban aerosol organic carbon concentrations in Beijing, Atmos. Environ.,
424 38, 1275-1282, <https://doi.org/10.1016/j.atmosenv.2003.11.037>, 2004.

425 Engling, G., Carrico, C.M., Kreidenweis, S.M., Collett Jr, J.L., Day, D.E., Malm, W.C., Lincoln, L.,
426 Hao, W.M., Iinuma, Y., and Herrmann, H.: Determination of levoglucosan in biomass
427 combustion aerosol by high-performance anion-exchange chromatography with pulsed
428 amperometric detection, Atmos. Environ., 40, S299-
429 S311, <https://doi.org/10.1016/j.atmosenv.2005.12.069>, 2006.

430 Engling, G., Lee, J. J., Tsai, Y. W., Lung, S. C. C., Chou, C. C. K., and Chan, C. Y.: Size resolved
431 anhydrosugar composition in smoke aerosol from controlled field burning of rice straw,
432 Aerosol Sci. Tech., 43, 662-672, <https://doi.org/10.1080/02786820902825113>, 2009.

433 Ge, B.Z., Wang, Z.F., Lin, W.L., Xu, X.B., Li, J., Ji, D.S., and Ma, Z.Q.: Air pollution over the north
434 china plain and its implication of regional transport: a new sight from the observed evidences,
435 Environ. Pollut., 166, 29-38, <https://doi.org/10.1016/j.envpol.2017.10.084>, 2017.

436 Gensch, I., Sang-Arlt, X.F., Laumer, W., Chan, C.Y., Engling, G., Rudolph, J., and Kiendler-Scharr, A.:
437 Using $\delta^{13}\text{C}$ of levoglucosan as a chemical clock, Environ. Sci.
438 Tech. <https://pubs.acs.org/doi/10.1021/acs.est.8b03054>, 2018.

439 He, K.B., Zhao, Q., Ma, Y.L., Duan, F.K., Yang, F.M., Shi, Z.B., and Chen, G.: Spatial and seasonal
440 variability of PM2.5 acidity at two Chinese megacities: insights into the formation of secondary
441 inorganic aerosols, Atmos. Chem. Phys., 12, 1377-1395, <https://doi.org/10.5194/acp-12-1377-2012>, 2012.

443 Hertwig, D., Burgin, L., Gan, C., Hort, M., Jones, A., Shaw, F., Witham, C., and Zhang, K.:
444 Development and demonstration of a Lagrangian dispersion modeling system for real-time
445 prediction of smoke haze pollution from biomass burning in Southeast Asia, J. Geophys. Res.:
446 Atmos., 120, 12605-12630, <https://doi.org/10.1002/2015JD023422>, 2015.

447 Ho, K.F., Engling, G., Sai Hang Ho, S., Huang, R., Lai, S., Cao, J., and Lee, S.C.: Seasonal
448 variations of anhydrosugars in PM2.5 in the Pearl River Delta Region, China, Tellus B, 66,
449 22577, <https://doi.org/10.3402/tellusb.v66.22577>, 2014.

450 Jung, J., Lee, S., Kim, H., Kim, D., Lee, H., and Oh, S.: Quantitative determination of the biomass-

burning contribution to atmospheric carbonaceous aerosols in Daejeon, Korea, during the rice-harvest period, *Atmos. Environ.*, 89, 642–650, <https://doi.org/10.1016/j.atmosenv.2014.03.010>, 2014.

Kanakidou, M., Seinfeld, J. H., Pandis, S. N., Barnes, I., Dentener, F. J., Facchini, M. C., Van Dingenen, R., Ervens, B., Nenes, A., Nielsen, C. J., Swietlicki, E., Putaud, J. P., Balkanski, Y., Fuzzi, S., Horth, J., Moortgat, G. K., Winterhalter, R., Myhre, C. E. L., Tsigaridis, K., Vignati, E., Stephanou, E. G., and Wilson, J.: Organic aerosol and global climate modelling: a review, *Atmos. Chem. Phys.*, 5, 1053–1123, <https://doi.org/10.5194/acp-5-1053-2005>, 2005.

Klejnowski, K., Janoszka, K., and Czaplicka, M.: Characterization and seasonal variations of organic and elemental carbon and levoglucosan in PM₁₀ in Krynica Zdroj, Poland, *Atmos.*, 8(10), 190, <https://doi.org/10.3390/atmos8100190>, 2017.

Kuang, Y., Xu, W.Y., Lin, W.L., Meng, Z.Y., Zhao, H. R., Ren, S.X., Zhang, G., Liang, L. L., and Xu, X. B.: Explosive morning growth phenomena of NH₃ on the North China Plain: Causes and potential impacts on aerosol formation, *Environ. Pollut.*, <https://doi.org/10.1016/j.envpol.2019.113621>, in press, 2020.

Lee, T., Sullivan, A.P., Mack, L., Jimenez, J.L., Kreidenweis, S.M., Onasch, T.B., Worsnop, D.R., Malm, W., Wold, C.E., Hao, W.M., and Collett Jr., J.L.: Chemical smoke marker emissions during flaming and smoldering phases of laboratory open burning of wildland fuels, *Aerosol Science and Technology* 44, <http://dx.doi.org/10.1080/02786826.2010.499884>, 2010.

Liang, L., Engling, G., Du, Z., Cheng, Y., Duan, F., Liu, X., and He, K.: Seasonal variations and source estimation of saccharides in atmospheric particulate matter in Beijing, China, *Chemosphere*, 150, 365–377, [10.1016/j.chemosphere.2016.02.002](https://doi.org/10.1016/j.chemosphere.2016.02.002), 2016.

Liang, L., Engling, G., Zhang, X., Sun, J., Zhang, Y., Xu, W., Liu, C., Zhang, G., Liu, X., and Ma, Q.: Chemical characteristics of PM 2.5 during summer at a background site of the Yangtze River Delta in China, *Atmospheric Research*, 198, 163–172, [10.1016/j.atmosres.2017.08.012](https://doi.org/10.1016/j.atmosres.2017.08.012), 2017.

Liang, L., Engling, G., Cheng, Y., Liu, X., Du, Z., Ma, Q., Zhang, X., Sun, J., Xu, W., Liu, C., Zhang, G., and Xu, H.: Biomass burning impacts on ambient aerosol at a background site in East China: Insights from a yearlong study, *Atmospheric Research*, 231, 104660, [10.1016/j.atmosres.2019.104660](https://doi.org/10.1016/j.atmosres.2019.104660), 2020.

Lin, W.L., Xu, X.B., Sun, J.Y., Liu, X.W., and Wang, Y.: Background concentrations of reactive gases and the impacts of long-range transport at the jinsha regional atmospheric background station, *Science China (Earth Sciences)*, 54, 1604–1613, 2011.

Liu, L., Liu, Y., Wen, W., Liang, L., Ma, X., Jiao, J., and Guo, K.: Source Identification of Trace Elements in PM2.5 at a Rural Site in the North China Plain, *Atmos.*, 11(2), 179, <https://doi.org/10.3390/atmos11020179>, 2020.

Meng, Z.Y., Xu, X.B., Lin, W. L., Ge, B.Z., Xie, Y.L., Song, B., Jia, S.H., Zhang, R., Peng, W., Wang, Y., Cheng, H.B., Yang, W., and Zhao, H.R.: Role of ambient ammonia in particulate ammonium formation at a rural site in the North China Plain, *Atmos. Chem. Phys.*, 18, 167–184, <https://doi.org/10.5194/acp-18-167-2018>, 2018.

Merico, E., Grasso, F.M., Cesari, D., Decesari, S., Belosi, F., Manarini, F., De Nuntiis, P., Rinaldi, M., Gambaro, A., Morabito, E., and Contini, D.: Characterisation of atmospheric pollution near an industrial site with a biogas production and combustion plant in southern Italy, <https://doi.org/10.1016/j.scitotenv.2020.137220>, *Sci. Tot. Environ.*, 717, 137220, 2020.

Mkoma, S. L., Kawamura, K., and Fu, P. Q.: Contributions of biomass/biofuel burning to organic aerosols and particulate matter in Tanzania, East Africa, based on analyses of ionic species, organic and elemental carbon, levoglucosan and mannosan, *Atmos. Chem. Phys.*, 13, 10325–10338, <https://doi.org/10.5194/acp-13-10325-2013>, 2013.

Peltier, R. E., Hecobian, A. H., Weber, R. J., Stohl, A., Atlas, E. L., Riemer, D. D., Blake, D. R.,

500 Apel, E., Campos, T., and Karl, T.: Investigating the sources and atmospheric processing of
501 fine particles from Asia and the Northwestern United States measured during INTEX B, *Atmos.*
502 *Chem. Phys.*, 8, 1835-1853, <https://doi.org/10.5194/acp-8-1835-2008>, 2008.

503 Pietrogrande, M.C., Bacco, D., Ferrari, S., Kaipainen, J., Ricciardelli, I., Riekkola, M.-L., Trentini,
504 A., and Visentin, M.: Characterization of atmospheric aerosols in the Po valley during the
505 supersito campaigns — Part 3: Contribution of wood combustion to wintertime atmospheric
506 aerosols in Emilia Romagna region (Northern Italy), *Atmos. Environ.*, 122, 291-
507 305, <https://doi.org/10.1016/j.atmosenv.2015.09.059>, 2015

508 Pope, C.A., and Dockery, D.W.: Health effects of fine particulate air pollution: lines that connect, *J.*
509 *Air Waste Manage.*, 56, 709-742, <https://doi.org/10.1080/10473289.2006.10464485>, 2006.

510 Sang, X.F., Zhang, Z.S., Chan, C.Y., and Engling, G.: Source categories and contribution of biomass
511 smoke to organic aerosol over the southeastern Tibetan plateau, *Atmos. Environ.*, 78, 113-
512 123, <https://doi.org/10.1016/j.atmosenv.2012.12.012>, 2013.

513 Sang, X.F., Gensch, I., Kammer, B., Khan, A., Kleist, E., Laumer, W., Schlag, P., Schmitt, S.H.,
514 Wildt, J., Zhao, R., Mungall, E.L., Abbatt, J.P.D., and Kiendler-Scharr, A.: Chemical stability
515 of levoglucosan: An isotopic perspective, *J. Geophys. Res.*, 43, 5419-
516 5424, <https://doi.org/10.1002/2016GL069179>, 2016.

517 Schkolnik, G., Falkovich, A.H., Rudich, Y., Maenhaut, W., and Artaxo, P.: New analytical method
518 for the determination of levoglucosan, polyhydroxy compounds, and 2-methylerythritol and its
519 application to smoke and rainwater samples, *Environ. Sci. Technol.*, 39, 2744-
520 2752, <https://doi.org/10.1021/es048363c>, 2005.

521 Shen, X.J., Sun, J.Y., Zhang, X.Y., Zhang, Y.M., Wang, Y.Q., Tan, K.Y., Wang, P., Zhang, L., Qi,
522 X.F., Che, H.Z., Zhang, Z., Zhong, J.T., Zhao, H.R., and Ren, S.X.: Comparison of submicron
523 particles at a rural and an urban site in the North China Plain during the December 2016 heavy
524 pollution episodes, *J. Meteorol. Res.*, 32, 14-25, <https://doi.org/10.1007/s13351-018-7060-7>,
525 2018.

526 Streets, D.G., Bond, T.C., Carmichael, G.R., Fernandes, S.D., Fu, Q., He, D., Klimont, Z., Nelson,
527 S.M., Tsai, N.Y., Wang, M.Q., Woo, J.H., and Yarber, K.F.: An inventory of gaseous and
528 primary aerosol emissions in Asia in the year 2000, *J. Geophys. Res.*, 108 (D21),
529 8809. <http://dx.doi.org/10.1029/2002JD003093>, 2003.

530 Sullivan, A.P., Holden, A.S., Patterson, L.A., McMeeking, G.R., Kreidenweis, S.M., Malm, W.C.,
531 Hao, W.M., Wold, C.E., and Collett Jr., J.L.: A method for smoke marker measurements and
532 its potential application for determining the contribution of biomass burning from wildfires
533 and prescribed fires to ambient PM_{2.5} organic carbon, *J. Geophys. Res.*, 113,
534 D22302, <https://doi.org/10.1029/2008JD010216>, 2008.

535 Sun, K., Liu, X.G., Gu, J.W., Li, Y.P., Qu, Y., An, J.L., Wang, J.L., Zhang, Y.H., Hu, M., Zhang, F.:
536 Chemical characterization of size-resolved aerosols in four seasons and hazy days in the
537 megacity Beijing of China, *J. Environ. Sci.*, 32, 155-
538 167, <https://doi.org/10.1016/j.jes.2014.12.020>, 2015.

539 Sun, Y.L., Wang, Z.F., Fu, P.Q., Yang, T., Jiang, Q., Dong, H.B., Li, J., and Jia, J.J.: Aerosol
540 composition, sources and processes during wintertime in Beijing, China, *Atmos. Chem. Phys.*,
541 13, 4577-4592, <https://doi.org/10.5194/acp-13-4577-2013>, 2013.

542 Sun, Y.L., Zhang, Q., Anastasio, C., and Sun, J.: Insights into secondary organic aerosol formed via
543 aqueous-phase reactions of phenolic compounds based on high resolution mass spectrometry,
544 *Atmos. Chem. Phys.*, 10, 4809-4822, <https://doi.org/10.5194/acp-10-4809-2010>, 2010.

545 Tan, J.H., Duan, J.C., Zhen, N.J., He, K.B., and Hao, J.M.: Chemical characteristics and source of
546 size-fractionated atmospheric particle in haze episode in Beijing, *Atmos. Res.*, 167, 24-
547 33, <https://doi.org/10.1016/j.atmosres.2015.06.015>, 2016.

548 Tang, R., Wu, Z., Li, X., Wang, Y., Shang, D., Xiao, Y., Li, M., Zeng, L., Wu, Z., Hallquist, M., Hu,

549 M., and Guo, S.: Primary and secondary organic aerosols in summer 2016 in Beijing, *Atmos.*
550 *Chem. Phys.*, 18, 4055-4068, <https://doi.org/10.5194/acp-18-4055-2018>, 2018.

551 Urban, R.C., Lima-Souza, M., Caetano-Silva, L., Queiroz, M.E.C., Nogueira, R.F.P., Allen, A.G.,
552 Cardoso, A.A., Held, G., and Campos, M.L. A.M.: Use of levoglucosan, potassium, and water-
553 soluble organic carbon to characterize the origins of biomass-burning aerosols, *Atmos.*
554 *Environ.*, 61, 562-569, <https://doi.org/10.1016/j.atmosenv.2012.07.082>, 2012.

555 Wang, Z., Wang, T., Guo, J., Gao, R., Xue, L.K., Zhang, J.M., Zhou, Y., Zhou, X.H., Zhang, Q.Z.,
556 and Wang, W.X., 2012. Formation of secondary organic carbon and cloud impact on
557 carbonaceous aerosols at Mount Tai, North China, *Atmos. Environ.*, 46, 516-
558 527, <https://doi.org/10.1016/j.atmosenv.2011.08.019>, 2012.

559 Wu, Y., Ge, X., Wang, J., Shen, Y., Ye, Z., Ge, S., Wu, Y., Yu, H., and Chen, M.: Responses of
560 secondary aerosols to relative humidity and photochemical activities in an industrialized
561 environment during late winter, *Atmospheric Environment*, 193, 66-78,
562 [10.1016/j.atmosenv.2018.09.008](https://doi.org/10.1016/j.atmosenv.2018.09.008), 2018.

563 Xu, W., Kuang, Y., Zhao, C., Tao, J., Zhao, G., Bian, Y., Yang, W., Yu, Y., Shen, C., Liang, L., Zhang,
564 G., Lin, W., and Xu, X.: NH₃-promoted hydrolysis of NO₂ induces explosive growth in HONO,
565 *Atmos. Chem. Phys.*, 19, 10557-10570, <https://doi.org/10.5194/acp-19-10557-2019>, 2019

566 Xu, W., Kuang, Y., Liang, L., He, Y., Cheng, H., Bian, Y., Tao, J., Zhang, G., Zhao, P., Ma, N., Zhao,
567 H., Zhou, G., Su, H., Cheng, Y., Xu, X., Shao, M., and Sun, Y.: Dust-Dominated Coarse
568 Particles as a Medium for Rapid Secondary Organic and Inorganic Aerosol Formation in
569 Highly Polluted Air, *Environ. Sci. Technol.*, 54, 15710-15721, [10.1021/acs.est.0c07243](https://doi.org/10.1021/acs.est.0c07243),
570 2020.Xu, X., Zhang, H., Lin, W., Wang, Y., Xu, W., and Jia, S.: First simultaneous
571 measurements of peroxyacetyl nitrate (PAN) and ozone at Nam Co in the central Tibetan
572 Plateau: impacts from the PBL evolution and transport processes, *Atmos. Chem. Phys.*, 18,
573 5199-5217, <https://doi.org/10.5194/acp-18-5199-2018>, 2018.

574 Yang, F.M., Tan, J.H., Zhao, Q., Du, Z.Y., He, K.B., Ma, Y.L., Duan, F.K., Chen, G., and Zhao, Q.:
575 Characteristics of PM_{2.5} speciation in representative megacities and across China, *Atmos.*
576 *Chem. Phys.*, 11, 5207-5219, <https://doi.org/10.5194/acp-11-5207-2011>, 2011.

577 Yao, L., Yang, L.X., Chen, J.M., Wang, X.F., Xue, L.K., Li, W.J., Sui, X., Wen, L., Chi, J.W., Zhu,
578 Y.H., Zhang, J.M., Xu, C.H., Zhu, T., and Wang, W.X.: Characteristics of carbonaceous
579 aerosols: Impact of biomass burning and secondary formation in summertime in a rural area of
580 the North China Plain, *Sci. Tot. Environ.*, 557-
581 558, <https://doi.org/10.1016/j.scitotenv.2016.03.111>, 2016.

582 Yu, J.T., Yan, C.Q., Liu, Y., Li, X.Y., Zhou, T., and Zheng, M.: Potassium: A Tracer for Biomass
583 Burning in Beijing? *Aerosol Air Qual. Res.*, 18, 2447-2459, doi: 10.4209/aaqr.2017.11.0536,
584 2018.

585 Zhang, T., Cao, J.J., Chow, J.C., Shen, Z.X., Ho, K.F., Ho, S.S.H., Liu, S.X., Han, Y.M., Watson,
586 J.G., Wang, G.H., and Huang, R.J.: Characterization and seasonal variations of levoglucosan
587 in fine particulate matter in Xi'an, China, *J. Air Waste Manage.*, 64, 1317-
588 1327, <https://doi.org/10.1080/10962247.2014.944959>, 2014.

589 Zhang, T., Claeys, M., Cachier, H., Dong, S.P., Wang, W., Maenhaut, W., and Liu, X.D.:
590 Identification and estimation of the biomass burning contribution to Beijing aerosol using
591 levoglucosan as a molecular marker, *Atmos. Environ.*, 42, 7013-
592 7021, <https://doi.org/10.1016/j.atmosenv.2008.04.050>, 2008.

593 Zhang, Z., Engling, G., Lin, C.-Y., Chou, C. C. K., Lung, S.-C. C., Chang, S.-Y., Fan, S., Chan, C.-
594 Y., and Zhang, Y.-H.: Chemical speciation, transport and contribution of biomass burning
595 smoke to ambient aerosol in Guangzhou, a mega city of China, *Atmospheric Environment*, 44,
596 3187-3195, [10.1016/j.atmosenv.2010.05.024](https://doi.org/10.1016/j.atmosenv.2010.05.024), 2010.

597 Zhang, Z., Gao, J., Engling, G., Tao, J., Chai, F., Zhang, L., Zhang, R., Sang, X., Chan, C.Y., Lin,
598 Z., and Cao, J.: Characteristics and applications of size-segregated biomass burning tracers in

599 China's Pearl River Delta region, *Atmos. Environ.*, 102, 290-
600 301, <https://doi.org/10.1016/j.atmosenv.2014.12.009>, 2015.

601 Zheng, G.J., Duan, F.K., Su, H., Ma, Y.L., Cheng, Y., Zheng, B., Zhang, Q., Huang, T., Kimoto, T.,
602 Chang, D., Pöschl, U., Cheng, Y. F., and He, K. B.: Exploring the severe winter haze in Beijing:
603 the impact of synoptic weather, regional transport and heterogeneous reactions, *Atmos. Chem.
604 Phys.*, 15, 2969-2983, <https://doi.org/10.5194/acp-15-2969-2015>, 2015.

605 Zheng, M., Salmon, L. G., Schauer, J. J., Zeng, L., Kiang, C. S., Zhang, Y., and Cass, G. R.: Seasonal
606 trends in PM_{2.5} source contributions in Beijing, China, *Atmos. Environ.*, 39, 3967-
607 3976, <https://doi.org/10.1016/j.atmosenv.2005.03.036>, 2005.

608 Zhong, J.T., Zhang, X.Y., and Wang, Y.Q.: Reflections on the threshold for PM_{2.5} explosive growth
609 in the cumulative stage of winter heavy aerosol pollution episodes (HPEs) in Beijing, *Tellus B*,
610 71, 1-7, <https://doi.org/10.1080/16000889.2018.1528134>, 2019.

611 Zhong, J.T., Zhang, X.Y., Wang, Y.Q., Liu, C., and Dong, Y.S.: Heavy aerosol pollution episodes in
612 winter Beijing enhanced by radiative cooling effects of aerosols, *Atmos. Res.*, 209, 59-
613 64, <https://doi.org/10.1016/j.atmosres.2018.03.011>, 2018.

614 Zhou, Y., Xing, X., Lang, J., Chen, D., Cheng, S., Wei, L., Wei, X., and Liu, C.: A comprehensive
615 biomass burning emission inventory with high spatial and temporal resolution in China, *Atmos.
616 Chem. Phys.*, 17, 2839-2864, 10.5194/acp-17-2839-2017, 2017.

617 Zhu, C., Kawamura, K., and Kunwar, B.: Effect of biomass burning over the western North Pacific
618 Rim: wintertime maxima of anhydrosugars in ambient aerosols from Okinawa, *Atmos. Chem.
619 Phys.*, 15, 1959-1973, <https://doi.org/10.5194/acp-15-1959-2015>, 2015.

620 Zhu, Y.H., Yang, L.X., Kawamura, K., Chen, J.M., Ono, K., Wang, X.F., Xue, L.K., and Wang, W.X.:
621 Contributions and source identification of biogenic and anthropogenic hydrocarbons to
622 secondary organic aerosols at Mt. Tai in 2014, *Environ. Pollut.*, 220, 863-
623 872, <https://doi.org/10.1016/j.envpol.2016.10.070>, 2017.

624

625

626

627

628

629

630

631

632

633

634

635

636

637

638

639

640

641 **Table 1.** Average concentrations and the range of $\text{PM}_{2.5\text{-cal}}$ and its chemical components, biomass burning
 642 tracers ($\mu\text{g m}^{-3}$), gaseous species, ratios of OC/EC and levoglucosan /OC, as well as meteorological data
 643 observed at GC site at daytime, nighttime and whole day, respectively, during the sampling period from
 644 15 Oct to 23 Nov 2016.

| Species | Daytime (N = 34) | | Nighttime (N = 33) | | Whole period (N = 37)* | |
|------------------------------------|-----------------------|---------------|-----------------------|---------------|------------------------|-----------------|
| | Average concentration | Range | Average concentration | Range | Average concentration | Range |
| $\text{PM}_{2.5\text{-cal}}$ | 117 ± 58.8 | 19.0 - 225 | 170 ± 116 | 21.1 - 465 | 137 ± 72.4 | 23.3 - 319 |
| OC | 26.8 ± 15.7 | 3.78 - 64.8 | 61.6 ± 49.5 | 2.88 - 175 | 44.0 ± 31.0 | 4.13 - 117 |
| EC | 13.4 ± 8.49 | 1.44 - 34.0 | 30.9 ± 28.5 | 2.21 - 129 | 21.7 ± 15.8 | 2.46 - 74.9 |
| TC | 49.3 ± 27.6 | 5.76 - 124 | 92.5 ± 73.6 | 5.10 - 289 | 65.8 ± 44.1 | 7.36 - 192 |
| OC/EC | 2.02 ± 1.26 | 1.09 - 3.31 | 2.25 ± 1.04 | 1.04 - 6.72 | 1.95 ± 0.60 | 0.83 - 3.10 |
| SO_4^{2-} | 12.1 ± 9.31 | 1.65 - 39.7 | 9.02 ± 6.22 | 1.55 - 23.2 | 10.5 ± 6.87 | 1.66 - 29.5 |
| NO_3^- | 16.9 ± 9.96 | 1.85 - 41.2 | 13.1 ± 8.52 | 1.56 - 38.0 | 15.9 ± 9.29 | 2.40 - 45.2 |
| Cl^- | 4.33 ± 2.30 | 0.82 - 9.46 | 6.08 ± 4.00 | 0.62 - 16.0 | 4.90 ± 2.46 | 0.93 - 9.37 |
| NH_4^+ | 11.7 ± 6.76 | 1.84 - 26.0 | 10.0 ± 5.75 | 1.33 - 22.2 | 10.9 ± 5.51 | 1.99 - 25.4 |
| K^+ | 1.43 ± 0.54 | 0.20 - 2.64 | 1.78 ± 0.95 | 0.22 - 4.19 | 1.52 ± 0.62 | 0.50 - 2.96 |
| Mg^{2+} | 0.26 ± 0.14 | 0.07-0.64 | 0.19 ± 0.09 | 0.06 - 0.38 | 0.14 ± 0.12 | 0.04 - 0.43 |
| Ca^{2+} | 2.24 ± 1.01 | 1.02-4.75 | 1.56 ± 0.08 | 0.77 - 3.56 | 1.54 ± 0.90 | 0.49 - 3.84 |
| Na^+ | 0.44 ± 0.17 | 0.10 - 0.79 | 0.43 ± 0.24 | 0.10 - 1.31 | 0.42 ± 0.17 | 0.11 - 0.88 |
| $\text{NO}_3^- / \text{SO}_4^{2-}$ | 1.67 ± 0.82 | 0.75 - 5.52 | 1.54 ± 0.57 | 0.74 - 3.50 | 1.65 ± 0.62 | 0.78 \pm 3.96 |
| Levoglucosan | 0.57 ± 0.62 | 0.05 - 3.74 | 1.10 ± 0.99 | 0.05 - 4.82 | 0.79 ± 0.75 | 0.14 - 4.37 |
| Mannosan | 0.024 ± 0.023 | 0.00 - 0.14 | 0.05 ± 0.04 | 0.00 - 0.21 | 0.03 ± 0.03 | 0.00 - 0.18 |
| levoglucosan/OC | 0.018 ± 0.011 | 0.005 - 0.067 | 0.020 ± 0.010 | 0.004 - 0.047 | 0.020 ± 0.009 | 0.006 - 0.045 |
| NO (ppb) | 23.0 ± 14.7 | 2.07 - 56.0 | 45.9 ± 29.5 | 1.59 - 96.9 | 31.8 ± 18.3 | 1.81 - 68.5 |
| NO_2 (ppb) | 25.8 ± 10.4 | 8.18 - 51.6 | 29.3 ± 9.37 | 8.81 - 51.1 | 26.6 ± 8.74 | 8.62 - 51.4 |
| SO_2 (ppb) | 9.78 ± 4.96 | 3.11 - 22.5 | 9.63 ± 5.67 | 2.91 - 28.7 | 8.61 ± 4.04 | 3.37 - 20.4 |
| CO (ppm) | 0.96 ± 0.73 | 0.03 - 2.49 | 1.29 ± 1.04 | 0.02 - 3.26 | 1.05 ± 0.76 | 0.12 - 2.48 |
| O_3 (ppb) | 13.0 ± 9.10 | 1.42 - 41.84 | 5.00 ± 5.73 | 1.60 - 24.30 | 9.25 ± 5.78 | 1.67 - 24.0 |
| NH_3 (ppb) | 16.4 ± 11.3 | 1.68 - 46.2 | 18.3 ± 10.7 | 1.03 - 42.7 | 17.1 ± 9.88 | 1.46 - 44.4 |
| Temperature (°C) | 7.71 ± 4.01 | - 2.07-15.9 | 3.30 ± 4.69 | - 6.60 - 14.5 | 6.95 ± 4.58 | - 4.33 - 15.4 |
| Relative Humidity (%) | 68 ± 17 | 31 - 98 | 85 ± 14 | 34 - 100 | 77 ± 13 | 48 - 99 |
| Wind speed (m s ⁻¹) | 1.43 ± 1.17 | 0.09 - 5.65 | 0.79 ± 1.55 | 0.03 - 7.19 | 1.07 ± 1.14 | 0.04 - 5.02 |

645 * Six whole-day samples were included in the data analysis of the “Whole period”.

646

647

648

649

650

651

652 **Table 2.** Concentrations of chemical components in PM_{2.5} aerosols as well as their ratios and gaseous
 653 species collected at the GC site, during the four biomass burning periods (i.e., Minor, Intensive, Major
 654 and Heating period) from 15 Oct to 23 Nov 2016.

| Species | Period I (15-30 Oct) | Period II (31 Oct) | Period III (1 -14, Nov) | Period IV (15 -23, Nov) | |
|--|-----------------------------------|---------------------------------------|-----------------------------------|---|------|
| | Minor BB Average concentration | Intensive BB Average concentration | Major BB Average concentration | Heating period Average concentration | |
| PM _{2.5} -cal | 81.0 ± 44.5 | 235 | 2.91 | 163 ± 46.7 | 2.01 |
| Levoglucosan | 0.36 ± 0.14 | 4.37 | 12.1 | 0.90 ± 0.37 | 2.50 |
| Mannosan | 0.015 ± 0.005 | 0.18 | 12.0 | 0.038 ± 0.015 | 2.53 |
| OC | 16.2 ± 7.52 | 96.3 | 5.93 | 55.2 ± 17.1 | 3.41 |
| EC | 12.2 ± 5.85 | 36.0 | 2.96 | 25.5 ± 10.1 | 2.09 |
| TC | 28.4 ± 13.1 | 132 | 4.66 | 80.9 ± 34.6 | 2.85 |
| SO ₄ ²⁻ | 10.3 ± 8.96 | 4.56 | 0.44 | 11.8 ± 6.02 | 1.15 |
| NO ₃ ⁻ | 16.6 ± 12.9 | 18.1 | 1.09 | 16.5 ± 6.42 | 0.99 |
| NH ₄ ⁺ | 10.1 ± 7.40 | 10.0 | 0.99 | 12.0 ± 4.35 | 1.19 |
| K ⁺ | 1.16 ± 0.36 | 2.61 | 2.25 | 1.76 ± 0.46 | 1.52 |
| Cl ⁻ | 3.46 ± 1.97 | 7.49 | 2.16 | 5.58 ± 2.16 | 1.61 |
| OC/EC | 1.53 ± 0.35 | 2.67 | 1.75 | 2.31 ± 0.59 | 1.51 |
| NO ₃ ⁻ / SO ₄ ²⁻ | 1.74 ± 0.60 | 3.96 | 2.28 | 1.50 ± 0.35 | 0.86 |
| levoglucosan/OC | 0.025 ± 0.008 | 0.045 | 1.80 | 0.016 ± 0.005 | 0.64 |
| levoglucosan/EC | 0.039 ± 0.019 | 0.121 | 3.10 | 0.038 ± 0.017 | 0.97 |
| levoglucosan/ mannosan | 24.9 ± 4.44 | 24.1 | 0.97 | 24.8 ± 6.46 | 1.00 |
| levoglucosan/K ⁺ | 0.36 ± 0.081 | 1.67 | 4.64 | 0.51 ± 0.16 | 1.42 |
| NO (ppb) | 21.7 ± 12.5 | 21.7 | 1.00 | 39.6 ± 15.4 | 1.82 |
| NO ₂ (ppb) | 21.8 ± 4.95 | 26.5 | 1.22 | 32.7 ± 7.27 | 1.50 |
| NO _x (ppb) | 43.6 ± 16.3 | 48.2 | 1.11 | 72.4 ± 17.8 | 1.66 |
| SO ₂ (ppb) | 5.83 ± 2.46 | 8.04 | 1.38 | 11.1 ± 4.10 | 1.90 |
| CO (ppm) | 0.44 ± 0.33 | 0.70 | 1.59 | 1.65 ± 0.53 | 3.75 |
| O ₃ (ppb) | 9.79 ± 4.88 | 23.2 | 2.37 | 7.51 ± 3.87 | 0.77 |
| NH ₃ (ppb) | 14.3 ± 6.12 | 11.1 | 0.78 | 18.6 ± 8.03 | 1.30 |

655 *: indicates that the ratios of the heating period, intense BB period or major biomass burning period
 656 were divided by those from the minor BB period.

657

658

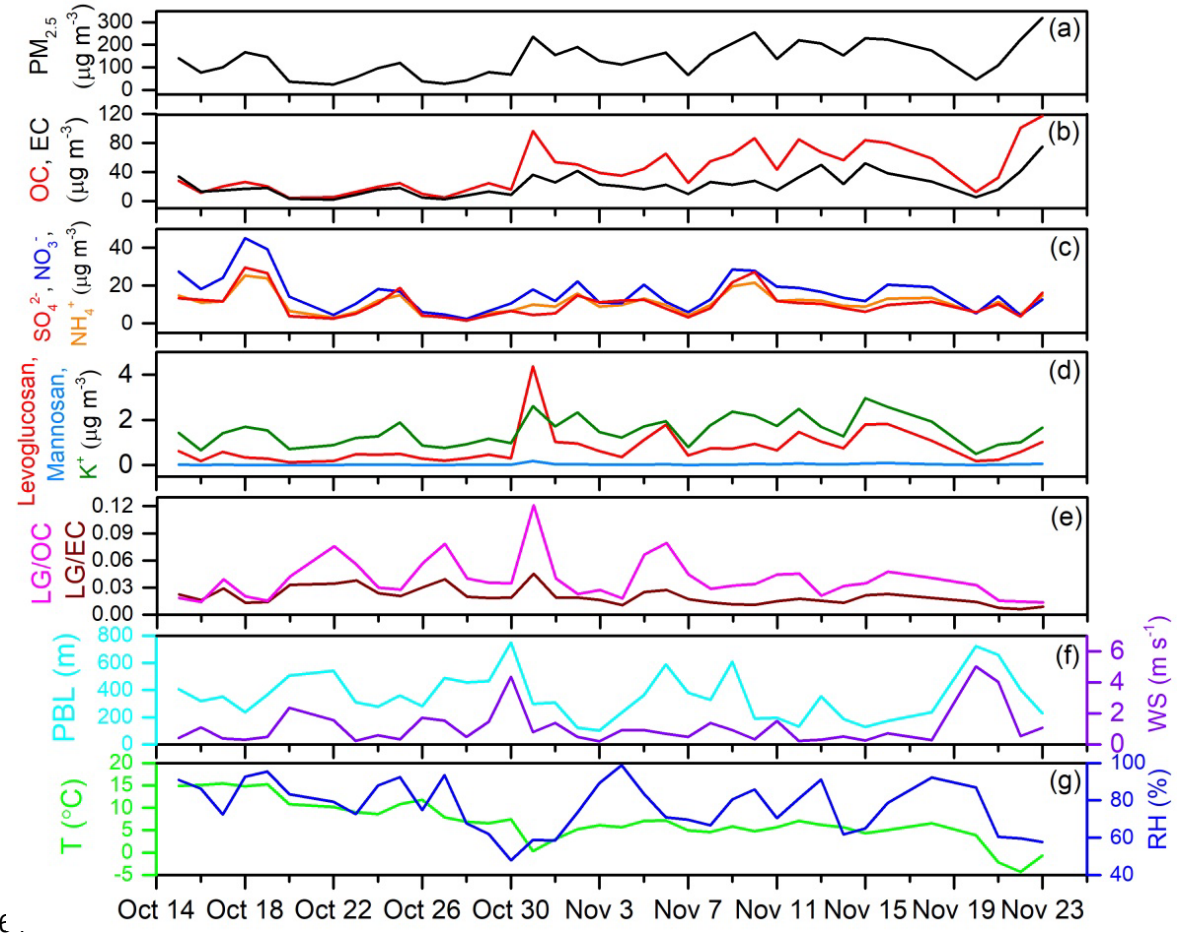
659

660

661

662

663



665 **Figure 1.** Time-series variation obtained for $\text{PM}_{2.5\text{-cal}}$ and its major components, biomass burning tracers
 666 as well as meteorological factors at the GC site during the sampling period from 15 Oct to 23 Nov 2016.
 667 (a) $\text{PM}_{2.5\text{-cal}}$, (b) OC and EC, (c) secondary inorganic aerosols, i.e., SO_4^{2-} , NO_3^- and NH_4^+ , (d)
 668 levoglucosan, mannosan and K^+ , (e) ratios of levoglucosan to OC (LG/OC) and levoglucosan to EC
 669 (LG/EC), (f) PBL and wind speed (WS), (g) temperature (T) and relative humidity (RH).

670

671

672

673

674

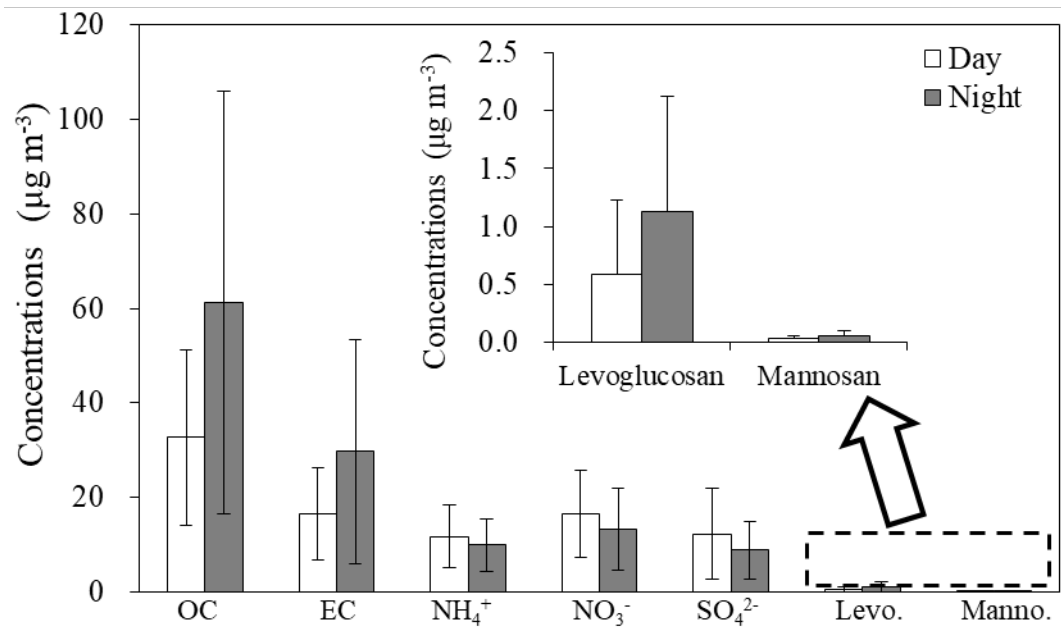
675

676

677

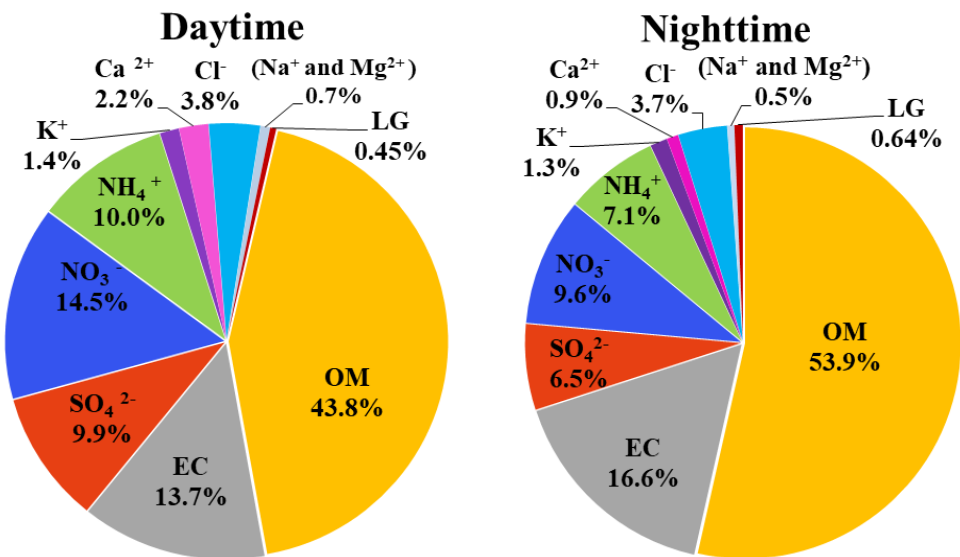
678

679



680
681 **Figure 2.** Day and night distributions of mean concentrations of main chemical components (OC, EC,
682 SO_4^{2-} , NO_3^- and NH_4^+) and biomass burning tracers (levoglucosan and mannosan) in $\text{PM}_{2.5}$ observed at
683 GC site during the sampling period.

684
685
686
687
688
689
690
691
692
693
694
695
696
697
698
699
700
701



702

703 **Figure 3.** Percent contributions of individual component mass concentrations to total estimated $\text{PM}_{2.5\text{-cal}}$
 704 mass in daytime and nighttime during the sampling period.

705

706

707

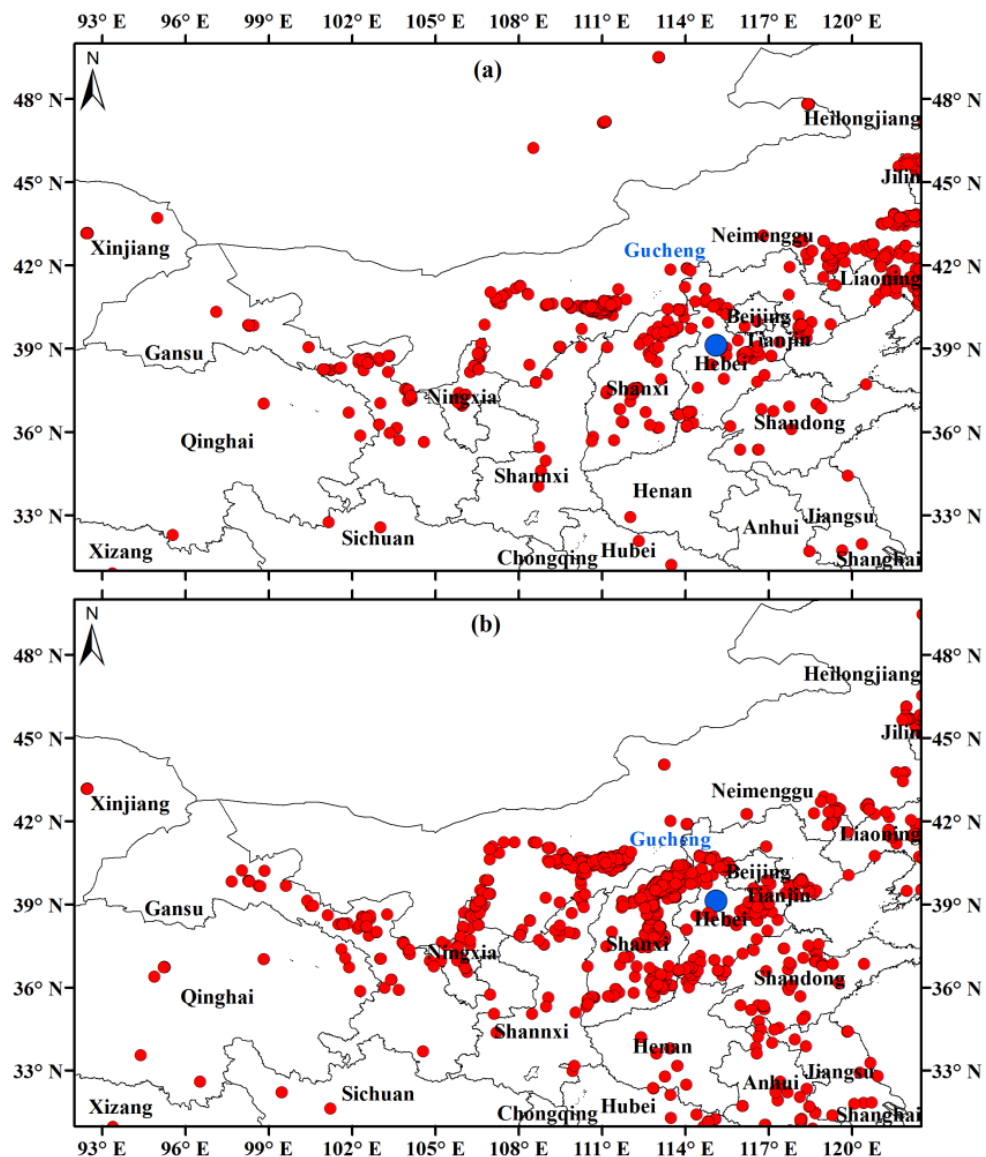
708

709

710

711

712



713

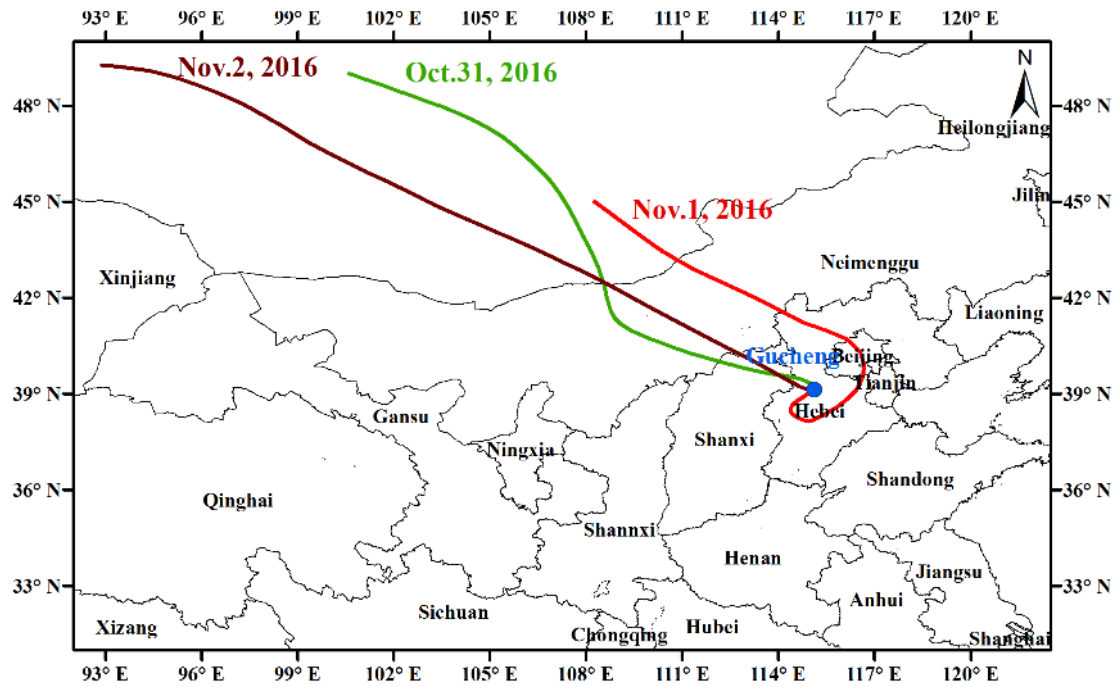
714 **Figure 4.** Fire spots at GC site and the surrounding provinces from (a) 15-30 October, 2016 and (b) 1 -
 715 23, November, 2016, observed by MODIS Terra satellites (blue dot is GC station).

716

717

718

719



720

721 **Figure 5.** 48 h back trajectories at 500 m at GC site ($39^{\circ}09'N$, $115^{\circ}44'E$) at 00:00 (UTC time) from 31
 722 October to 2 November, 2016.

723

724

725

726

727

728

729

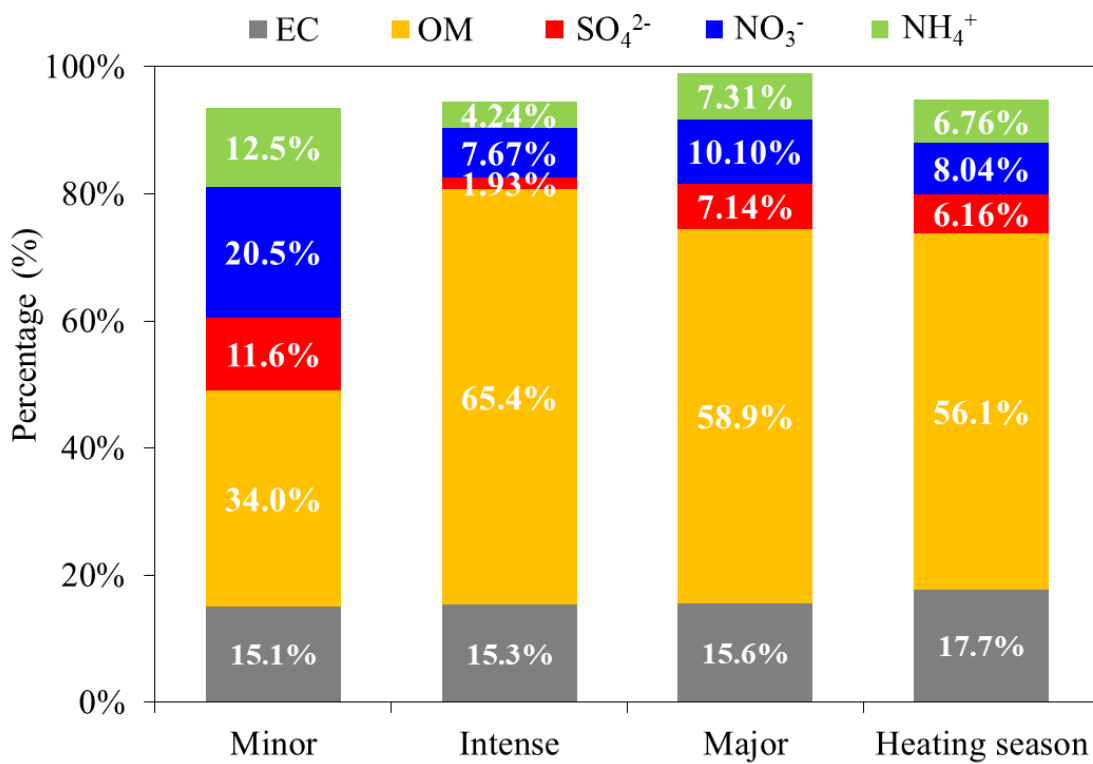
730

731

732

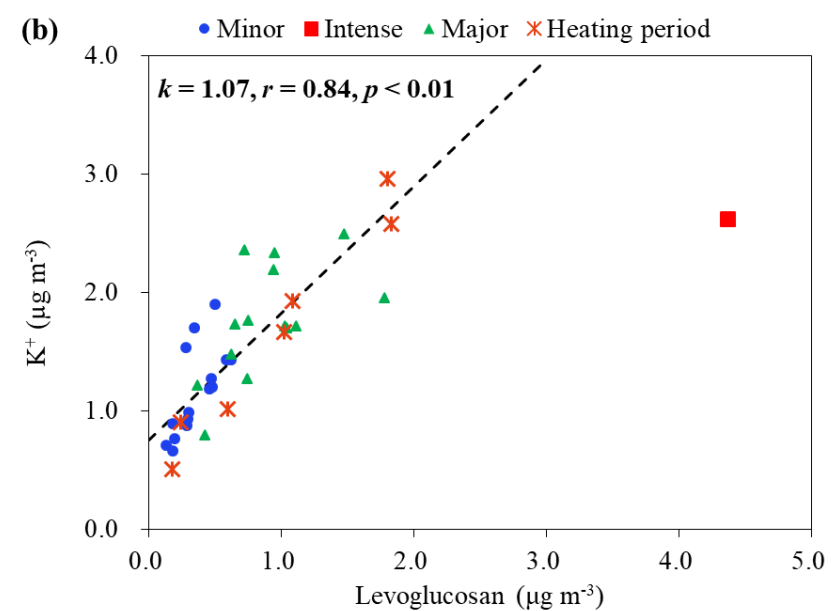
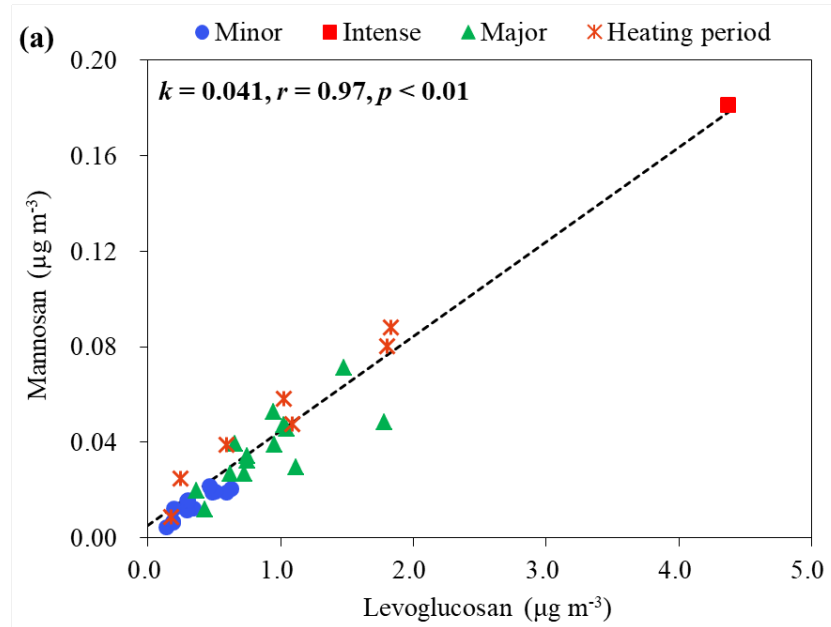
733

734



735
736 **Figure 6.** Mean percentiles of major components in PM_{2.5} with respect to different biomass burning
737 pollution periods at GC site during the sampling time.

738
739
740
741
742
743
744
745
746
747
748
749
750
751
752
753



756 **Figure 7.** Scatter plots of (a) levoglucosan versus mannosan, (b) levoglucosan versus K^+ . Statistical
757 analysis of sampling data was conducted with the linear fitting method.

758

759

760

761

762

763

764